Monitoring seasonal variations in surface wave velocity and groundwater levels in Western Australia using borehole ambient seismic noise interferometry

Leiyu He[1,2], Erdinc Saygin[2,3], David Lumley[2,4], Chaoying Bai[1]

[1]Department of Geophysics, Chang'an University, Xi'an, China
[2]Department of Physics, The University of Western Australia, Perth, Australia
[3]Deep Earth Imaging, Future Science Platform, CSIRO, Perth, Australia
[4]School of Natural Sciences and Mathematics, University of Texas at Dallas, Dallas, USA

Key Points:

- We use seismic noise recorded in a borehole to monitor changes of surface wave velocity using interferometric analysis at the SW Hub.
- We find that the change in seismic surface wave velocity is seasonal and strongly correlated with changes in groundwater levels.
- We propose that the change to rock density and shear velocity, are the main cause for the surface wave relative velocity changes observed.

Corresponding author: Leiyu He, leiyuhe@chd.edu.cn

Abstract

In order to explore the effects of environmental subsurface changes on seismic velocities, we use nearly four years (2015-2018) of continuous ambient seismic noise data recorded in a multi-level borehole to measure relative seismic surface wave velocity changes at the SW Hub CO_2 Geosequestration Site using seismic noise interferometry. We find a direct correlation between seismic velocity and seasonal groundwater changes, where seismic velocity changes follow groundwater level changes. We propose that the change to rock density and shear velocity, caused by groundwater saturation change, is consistent with and explains the data well.

Plain Language Summary

Groundwater resources are extremely important for society. In the context of global climate change, human activities have greatly changed the distribution and utilization potential of groundwater resources. Dynamic monitoring of groundwater level changes is of great significance for the rational use and protection of groundwater resources. By analyzing the ambient seismic noise recorded with geophones, we show that we can indirectly monitor the changes in groundwater level in Western Australia. We find that the velocity change curve is highly correlated with the groundwater level change. Our analyses show that it is feasible to use ambient noise data to monitor groundwater level changes.

1 Introduction

The surface of the earth supports life on the earth, this essential space is known as the Critical Zone (CZ) (Brantley et al., 2007), because it is vital for ecosystems. The CZ is increasingly impacted by human activities, including land and groundwater use, so research on the CZ will be important to optimally manage the use of these resources. The role of ambient noise is increasingly important and gives us a new method to study the physical properties of the CZ.(Larose et al., 2015).

Ambient seismic noise has proven to be an extremely useful method and has been applied in many areas of seismology (Lecocq et al., 2014; Larose et al., 2015), where it has been used for imaging (Shapiro et al., 2005; Lin et al., 2008; Saygin & Kennett, 2010; Poli et al., 2012; Saygin & Kennett, 2012; Issa et al., 2017), and environmental monitoring (Mainsant et al., 2012; Minato et al., 2012; Froment et al., 2013).

Since seismic noise is continuous, repeatable and ubiquitous, it gives the opportunity to study temporal changes of the subsurface over time (Nakata et al., 2019). Recently, many studies use ambient seismic noise to measure relative seismic velocity changes (dv/v), such as groundwater level changes (Sens-Schönfelder & Wegler, 2006; Lecocq et al., 2017; Clements & Denolle, 2018; Yang et al., 2018; Kim & Lekic, 2019), temperature induced changes (Richter et al., 2014; Mao et al., 2019), earth tide variations (Hillers et al., 2015; Mao et al., 2019), subsurface changes from volcanic activity (Brenguier, Shapiro, et al., 2008; Bennington et al., 2018; De Plaen et al., 2019; Yates et al., 2019), stress variations caused by post-seismic relaxation (Brenguier, Campillo, et al., 2008; Hobiger et al., 2012; Obermann et al., 2014; Hillers et al., 2019), and other applications. Australia is generally considered a relatively stable continent (Johnston, 1994), although the northern part of the Australian continent is colliding with the Sunda plate at a rate of 50 - 75 mm/yr (Roberts & Bally, 2012).

The SW Hub Project is located in the South Perth Basin of Western Australia, approximately 110 km south of the state capital Perth. The project site combines different methods of capture and storage to reduce CO_2 emissions (Stalker et al., 2013). The project site represents a major carbon capture and storage (CCS) research effort, intend-

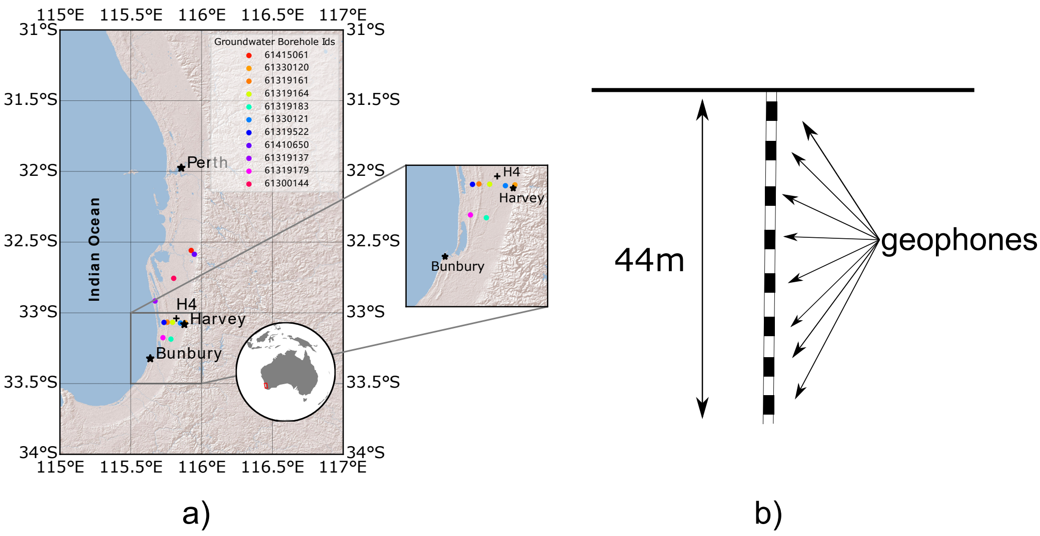

Figure 1. a) The map shows the location of the H4 seismic borehole well (black cross) and groundwater boreholes (circles). The location of the nearby cities are shown with stars, and the red rectangle in the inset map shows the location of the study area. b) The schematic of the borehole array. 3C geophones (black rectangles) are positioned at depths: 2, 8, 14, 20, 26, 32, 38 and 44 m (Lumley et al., 2015).

ing to store industrial CO_2 from coal-fired power plants, mineral processing facilities and other sources, in order to help meet Australia's national CO_2 emission reduction goals (Stalker et al., 2013). As a part of the project, in order to characterize natural environmental seismicity prior to any CO_2 injection, an eight-element 44 m deep seismic borehole was deployed and operated continuously with three-component sensors between 2015 and 2018 (Lumley et al., 2015).

The primary goal of this study is to explore the cause of seasonal seismic velocity changes (dv/v) observed at the SW Hub CO_2 Geosequestration Site borehole, by integrating continuous seismic noise recordings using interferometric analysis. The borehole array is approximately 17 km east of the Indian Ocean coast (Figure 1a), where highly energetic ocean seismic noise was recorded during the operation of the borehole. In our analyses, we integrate other environmental datasets such as groundwater, tidal, rainfall and temperature data to investigate whether there is an apparent correlation between these environmental phenomena and the observed seismic velocity changes.

2 Data and Methods

2.1 Data

The seismic data were recorded continuously at the SW Hub borehole array between August 2015 and April 2018 at a sampling rate of 1 kHz. The borehole comprises eight levels of three-component 10 Hz geophones of broad sensitivity range; with a vertical element spacing of 6 m (Figure 1b) where the deepest sensor element is located at 44 m. During the nearly three year operation of the borehole, there was only a limited amount of downtime of approximately five months in total.

2.2 Noise Cross-correlations & Measuring Seismic Velocity Changes

The cross-correlation operation can turn "noise" into a useful signal by providing an estimate of empirical Green's functions between seismic stations (Bensen et al., 2007). Most of the noise tomography results and time-lapse analyses are based on empirical Green's function retrieval (Nakata et al., 2019). Since ambient seismic noise is recorded continuously, these Green's functions can also be used to estimate the relative variations in velocities (Clarke et al., 2011).

We calculate three kinds of cross-correlation functions using all three components of the geophones: "vertical-vertical", "north-north", and "east-east". Daily cross-correlations of vertical-vertical, north-north and east-east components are calculated using a deconvolution technique (Helmberger & Wiggins, 1971), where the raw data is detrended (remove mean and trend) and a one hour correlation window with no overlap is used in the computations. For the end of each day, the resulting empirical Green's functions from each sensor pair are stacked to create a daily stacked Green's function. The whole suite of Green's function is shown in the Supporting Information (Figure S1).

After calculating the empirical Green's functions from the inter-element cross-correlations of the borehole for each day, we measure the relative velocity change by comparing each day's empirical Green's function with a reference Green's function created from the average of all Green's functions using the Moving Window Cross-Spectrum (MWCS) method of Clarke et al. (2011); Lecocq et al. (2014). The MWCS technique has the advantage of operating in the frequency domain, where the bandwidth of a coherent signal in the correlation function can be clearly defined (Clarke et al., 2011). This method calculates relative velocity changes by comparing the 'reference' Green's function with the 'observed' Green's function (Clarke et al., 2011).

In the calculations, we use both acausal and causal data time windows spanning from -4 to 4 s for the analysis windows for Green's functions. We also test the influence of user-selected parameters in the estimation of dv/v by trying different windows and step sizes. In the end, we use 0.2 s as the size of the moving window, and 0.04 s for the step size (20% of the window size), which yields robust and consistent measurements. Our test results show that velocity perturbation estimates are generally not sensitive to input parameters (i.e., window and step sizes; see Figure S5-S7), suggesting the robustness of our measurements. In order to ensure the accuracy of the calculations, and to eliminate the influence of noisy data segments, we only retain data with a coherency (mean coherence for each window) greater than 0.75 when calculating dv/v.

3 Results and Discussion

Since each sensor has three components, we calculated 84 (3x28) cross-correlation functions for all 28 possible combinations for each of the sensor components. For each cross-correlation function, we calculated the corresponding velocity change compared to the overall average. In Figures 2a-c, we plot the relative velocity changes measured at 1-5 Hz for different components (Z-Z, N-N, E-E), where each colored curve is the velocity curve for a different cross-correlation and the thick black line is the average curve for all combinations of sensor pairs. We calculate the sensitivity of Rayleigh waves between 1 and 5 Hz for a velocity model derived from Lumley et al. (2015) (See supporting information Figure S10). In this frequency range, phase velocities of Rayleigh waves are most sensitive to structure in the top 800 m. For comparison, we also calculated the relative velocity changes of other frequency ranges (See Figure S2 - S4 in Supporting information), it can be seen that the magnitude of the relative velocity changes at 1-5 Hz are the largest, followed by 5-10 Hz and 10-25 Hz as the smallest.

From Figures 2a-c we find that the dv/v curve has obvious seasonal and periodic variations ($\pm 0.5\%$ on average) and its wavelength of change is about one year. It reaches a negative maximum around September of each year and a positive maximum around April of the following year. These phenomena can be observed across all of the channel combinations of Z-Z, N-N, and E-E.

Figure 2d shows the Reduced Standing Water Level (RSWL: The elevation of the water level is calculated by subtracting the Depth to Water from a reference elevation) after normalization. Since there is no groundwater data available at the shallow seismic borehole, we select data from 11 nearby groundwater boreholes from Australian Groundwater Explorer that cover the majority of the recording duration from 2015 to 2018 in the vicinity of the seismic borehole. Given the different baselines of groundwater changes in each groundwater borehole, we normalize the data to identify the trends better. In addition, we provide the absolute groundwater data in the supporting information (Figure S8). The tidal variations, precipitation and the ambient air temperature are given in Figures 2e-g. We can also see that these environmental data exhibit a strong seasonal variation.

The general trend of groundwater variations in all of the 11 nearby wells is highly consistent (Figure 2d). The groundwater level change shows a high level of correlation with dv/v (Figure 2a-d). Previous studies have explored the relationship between surface wave (shear) velocity changes and groundwater level changes, one common observation found was that as groundwater levels rise, the dv/v will decrease, producing a clear negative correlation between the two parameters (Gassenmeier et al., 2014; Sens-Schönfelder & Wegler, 2006; Clements & Denolle, 2018). However, some studies have found that the relationship between them is positively correlated (Kim & Lekic, 2019), the primary reason behind the positive correlation is that auto-correlation method was used to calculate dv/v rather than cross-correlation, in this case dv/v is sensitive to the P wave velocity change. They modeled and found that rising groundwater levels will increase the P wave velocity.

We also observed a negative correlation in our analysis (Figures 2a-c). In October of 2015, the groundwater amplitude increases to a maximum, the result of increased precipitation during the rainy season, and in April of 2016, it drops to the minimum because of the lack of precipitation (2015.09 - 2016.04) (Commander, 2013). The patterns of change in other years are similar. The periodicity of groundwater variation is also about one year, equal to the wavelength of the change in dv/v. The correlation coefficient between mean dv/v and normalised mean RSWL is 0.928, indicating a significant likelihood that the change in surface wave shear dv/v is caused by groundwater level changes.

Large earthquakes can also cause changes in the velocity of the subsurface (Hobiger et al., 2012; Minato et al., 2012). However, this change rate is more instantaneous rather than seasonal periodicity, and we did not find evidence of earthquake activity with a Mw magnitude greater than 4.0, within 50 km of Harvey, during the analyses period. The variation of tide also exhibits a seasonal pattern (See Figure 2e). We calculate the correlation coefficient between mean dv/v and tide as 0.127. Mao et al. (2019) estimated the order of surface wave relative velocity variations induced by tide to be approximately around 0.01%, which is much smaller than the relative velocity variations that we observed. Consequently, we suggest that tidal variations are unlikely to be the primary cause of the seismic velocity changes.

The seismic velocities we observe do not show obvious correspondence with the temperature data unlike that observed by Richter et al. (2014). They reported a strong correlation between temperature and the induced seasonal velocity changes, but we have not observed this phenomenon (see Figure 2). If the velocity change is caused by temperature variations, a significant velocity change would have been observed within one day (Richter et al., 2014). We did not observe this phenomenon as shown in the diurnal plot (See Figure 3). The temperature-induced velocity change may be too small (less than 0.1%) and not easily observed (Yang et al., 2018; Richter et al., 2014; Clements &

Denolle, 2018; Tsai, 2011). One possible reason is that our geophones are located in a borehole, thus being at depth they are less affected by surface heat fluctations. We also calculate the correlation coefficient between dv/v and temperature as 0.400, which is much smaller than the groundwater correlation. In order to further explore the influence of temperature changes on the dv/v curve, we use the analytical model from Tsai (2011) to calculate the relative velocity change caused by temperature. Comparing the calculation results (See Figure S9 and Figure 2), we find that the effect of temperature is very small (less than 0.04%), which is not sufficient to influence the trend of the observed change. In summary, we conclude that temperature can not be a significant cause of the observed relative velocity changes. Interestingly, it can be seen from Figures 3a-c that the fluctuations between 00:00–10:00 UTC (8:00–18:00 local time) are significantly higher than at other times, which is likely caused by the result of an increase in human and farm animal (cattle) activity (noise) during daylight hours near the borehole.

In the previous discussion, we analyzed the effects of temperature and tide on relative seismic velocity changes. We conclude that these environmental phenomena are unlikely to be the cause of our relative velocity observations. Given the observed strong correlation coefficient between groundwater fluctations and velocity changes, we propose that the velocity changes in the SW Hub region are most likely to be caused by groundwater level changes. In the following sections, we propose a physical model to explain the correlation between groundwater saturation and seismic surface wave (shear) velocity.

Many previous studies argue that seismic velocity changes may result from the change in stress caused by changing groundwater levels. For example, Christensen and Wang (1985) found that an increase in pore pressure opens cracks and reduces the area of grain contact, thereby reducing seismic velocity. Clements and Denolle (2018) found that there is no statistically significant phase delay between dv/v and groundwater level changes, so the observed changes were attributed purely to the elastic response of the aquifer. Yang et al. (2018) suggested that bulk stress and pore pressure dominate the shallow subsurface, so the negative correlation between dv/v and groundwater level change should be attributed to the variations in the saturation and effective pressure. Tsai (2011) used a 2D model to calculate the theoretical velocity changes caused by thermoelastic stresses or hydrologic loading and suggested that the stress caused by groundwater level changes could be responsible for the velocity changes, since the velocity changes caused by direct elastic effect have a stronger and more robust signal than poroelastic and thermoelastic effect. Gassenmeier et al. (2014) suggested that increased saturation can cause a decrease in seismic velocity according to theory of Gassmann(Gassmann, 1951).

We describe the observed dv/v changes by inspecting the sensitivity of shear waves to fluid saturation, where in our study, the Rayleigh waves dominate the extracted Green's functions. The shear wave velocity (V_s) and saturated rock's density (ρ_{sat}) can be given as

$$V_s = \sqrt{\frac{G}{\rho}}, \tag{1}$$

$$\rho_{sat} = \rho_{dry} + \phi \rho_{water} S_w \tag{2}$$

where G is the shear modulus, (determined by the state of stress, the degree of cementation, and interparticle contacts such as capillary forces (Santamarina et al., 2005), and these factors can be affected by pore fluid pressure and saturation (Cho & Santamarina, 2001)), ρ is the mass density of the soil, where ϕ = porosity; $S_w = 0$ means no water in the pores and $S_w = 1$ means the pores are full of water.

Generally the shear modulus is often considered to be insensitive to fluid saturation (Bhuiyan & Holt, 2016). However, there are some laboratory studies that have found that the shear modulus of saturated rocks shows a very small reduction in comparison with dry rocks (Khazanehdari & Sothcott, 2003; Baechle et al., 2005). The mechanism of shear modulus change is complicated and could be attributed to the effects of fluid type, fluid viscosity, saturation, etc (Bhuiyan & Holt, 2016). These changes in properties can change the rock frame property through rock-fluid interaction and cause changes to the shear modulus (Baechle et al., 2005). As the saturation increases, the mass density increases. Therefore, an increase in saturation (increased groundwater level) causes a decrease in the velocity of the shear wave. We calculate the relative velocity change for various assumed conditions (See Figures S11-12), and show a clear decrease of V_s when the saturation increases. Cho and Santamarina (2001) observed this phenomenon; that as the water saturation increases, the shear wave velocity will gradually decrease. This corresponds well with the phenomenon we observed as the groundwater level rises and the dv/v decreases.

4 Conclusions

In this study, we use continuous seismic borehole data to calculate surface wave velocity changes in the SW Hub area. We found that the curves of the velocity changes are similar at different frequencies, but that their amplitudes are different. In order to explore the observed relative seismic velocity changes, we study four environmental data variables collected in the vicinity of the seismic borehole. We rule out the influence of temperature and tide on seismic velocity changes, since the observed changes at SW Hub are significantly larger than, and out of phase with, these effects. The change of groundwater level has a strong correlation (93%) with the dv/v curve, and Combined with a mathematical model for shear wave velocity change with saturation, we propose that the observed surface wave relative velocity change is caused by the changes in groundwater level. We propose that an increase in near surface groundwater level will cause an increase in water saturation, which will significant decreases to the rock bulk density, and possible modest decreases to the shear modulus, thereby reducing the shear velocity of the surface wave. Our research further shows that it is feasible to detect and monitor changes in groundwater level with passive seismic ambient noise data, which may be useful for future studies of groundwater resources and the critical zone.

Acknowledgments

Leiyu He thanks CSC (China Scholarship Council) for funding. ObsPy, MsNoise packages were used in the processing of the seismic data. We thank the Department of Transport of Australia for the tidal data. We also thank the Bureau of Meteorology of Australia for providing us rainfall, temperature and groundwater data. We thank Yunfeng Chen and Caroline Johnson for reviewing an earlier version of the manuscript. The authors wish to acknowledge financial assistance provided through Australian National Low Emissions Coal Research and Development (ANLEC R&D). ANLEC R&D is supported by Australian Coal Association Low Emissions Technology Limited and the Australian Government through the Clean Energy Initiative.

References

Baechle, G. T., Weger, R. J., Eberli, G. P., Massaferro, J. L., & Sun, Y.-F. (2005). Changes of shear moduli in carbonate rocks: Implications for gassmann applicability. *The Leading Edge*, *24*(5), 507–510.

Bennington, N., Haney, M., Thurber, C., & Zeng, X. (2018). Inferring magma dynamics at veniaminof volcano via application of ambient noise. *Geophysical Research Letters*, *45*(21), 11–650.

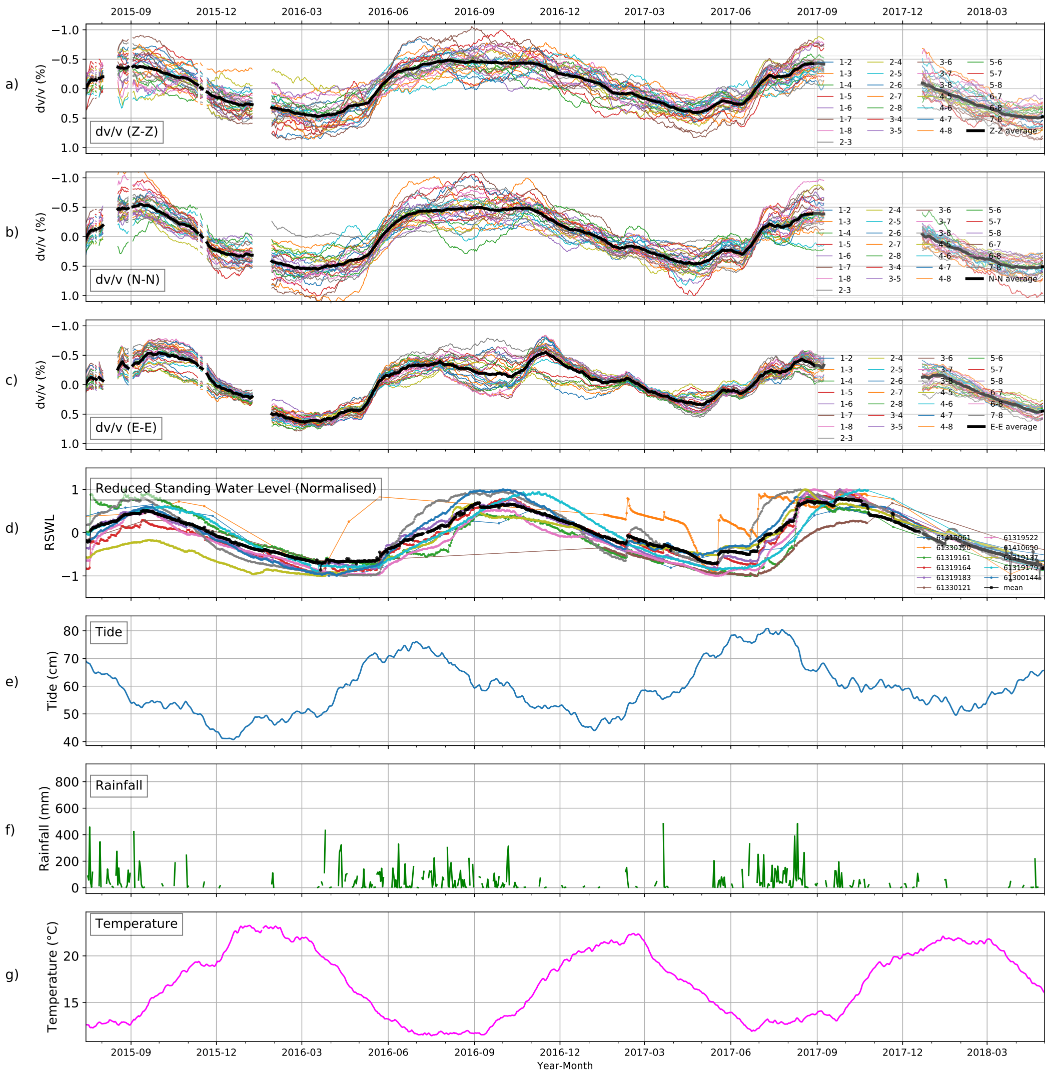

Figure 2. a) Relative velocity change as a function of time for Z-Z (1-5 Hz), the thick black line is the result after averaging all of the 28 curves. b) Same as a, but for N-N. c) Same as a, but for E-E. d) Reduced standing groundwater levels after normalization at ten wells near Harvey, their positions are in Figure 1. e) Sea level data at Bunbury. f) The rainfall plot of Bunbury. g) Temperature data at Bunbury.

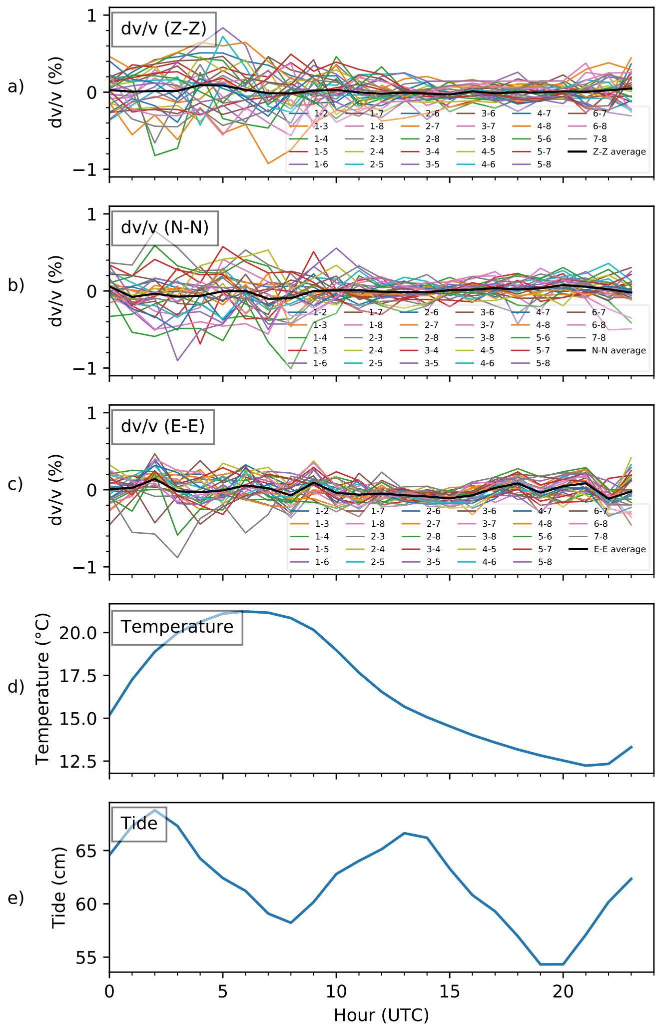

Figure 3. a) Relative velocity changes for Z-Z component in one day (1-5 Hz). b) Same as a), but for N-N component. c) Same as a), but for E-E component. d) Air temperature changes in one day. e) Sea level changes in 24 hours.

Bensen, G., Ritzwoller, M., Barmin, M., Levshin, A., Lin, F., Moschetti, M., ... Yang, Y. (2007). Processing seismic ambient noise data to obtain reliable broad-band surface wave dispersion measurements. *Geophysical Journal International*, *169*(3), 1239–1260.

Bhuiyan, M., & Holt, R. (2016). Variation of shear and compressional wave modulus upon saturation for pure pre-compacted sands. *Geophysical Journal International*, *206*(1), 487–500.

Brantley, S. L., Goldhaber, M. B., & Ragnarsdottir, K. V. (2007). Crossing disciplines and scales to understand the critical zone. *Elements*, *3*(5), 307–314.

Brenguier, F., Campillo, M., Hadziioannou, C., Shapiro, N., Nadeau, R. M., & Larose, E. (2008). Postseismic relaxation along the san andreas fault at parkfield from continuous seismological observations. *science*, *321*(5895), 1478–1481.

Brenguier, F., Shapiro, N. M., Campillo, M., Ferrazzini, V., Duputel, Z., Coutant, O., & Nercessian, A. (2008). Towards forecasting volcanic eruptions using seismic noise. *Nature Geoscience*, *1*(2), 126.

Cho, G. C., & Santamarina, J. C. (2001). Unsaturated particulate materials—particle-level studies. *Journal of geotechnical and geoenvironmental engineering*, *127*(1), 84–96.

Christensen, N., & Wang, H. (1985). The influence of pore pressure and confining pressure on dynamic elastic properties of berea sandstone. *Geophysics*, *50*(2), 207–213.

Clarke, D., Zaccarelli, L., Shapiro, N., & Brenguier, F. (2011). Assessment of resolution and accuracy of the moving window cross spectral technique for monitoring crustal temporal variations using ambient seismic noise. *Geophysical Journal International*, *186*(2), 867–882.

Clements, T., & Denolle, M. A. (2018). Tracking groundwater levels using the ambient seismic field. *Geophysical Research Letters*, *45*(13), 6459–6465.

Commander, D. P. (2013). *Groundwater resources of the lesueur carbon storage project area (sw hub).* Department of Mines and Petroleum.

De Plaen, R. S., Cannata, A., Cannavo, F., Caudron, C., Lecocq, T., & Francis, O. (2019). Temporal changes of seismic velocity caused by volcanic activity at mt. etna revealed by the autocorrelation of ambient seismic noise. *Frontiers in Earth Science*, *6*, 251.

Froment, B., Campillo, M., Chen, J., & Liu, Q. (2013). Deformation at depth associated with the 12 may 2008 mw 7.9 wenchuan earthquake from seismic ambient noise monitoring. *Geophysical Research Letters*, *40*(1), 78–82.

Gassenmeier, M., Sens-Schönfelder, C., Delatre, M., & Korn, M. (2014). Monitoring of environmental influences on seismic velocity at the geological storage site for co2 in ketzin (germany) with ambient seismic noise. *Geophysical Journal International*, *200*(1), 524–533.

Gassmann, F. (1951). Uber die elastizitat poroser medien: Vierteljahrsschrift der naturforschenden gesellschaft in zurich.

Helmberger, D., & Wiggins, R. A. (1971). Upper mantle structure of midwestern united states. *Journal of Geophysical Research*, *76*(14), 3229–3245.

Hillers, G., Campillo, M., Brenguier, F., Moreau, L., Agnew, D., & Ben-Zion, Y. (2019). Seismic velocity change patterns along the san jacinto fault zone following the 2010 m 7.2 el mayor-cucapah and m 5.4 collins valley earthquakes. *Journal of Geophysical Research: Solid Earth*, *124*(7), 7171–7192.

Hillers, G., Retailleau, L., Campillo, M., Inbal, A., Ampuero, J.-P., & Nishimura, T. (2015). In situ observations of velocity changes in response to tidal deformation from analysis of the high-frequency ambient wavefield. *Journal of Geophysical Research: Solid Earth*, *120*(1), 210–225.

Hobiger, M., Wegler, U., Shiomi, K., & Nakahara, H. (2012). Coseismic and post-seismic elastic wave velocity variations caused by the 2008 iwate-miyagi nairiku earthquake, japan. *Journal of Geophysical Research: Solid Earth*, *117*(B9).

Issa, N. A., Lumley, D., & Pevzner, R. (2017). Passive seismic imaging at reservoir depths using ambient seismic noise recorded at the otway co2 geological storage research facility. *Geophysical Journal International*, *209*(3), 1622–1628.

Johnston, A. (1994). *The earthquakes of stable continental regions* (Vol. 1). Electric Power Research Institute.

Khazanehdari, J., & Sothcott, J. (2003). Variation in dynamic elastic shear modulus of sandstone upon fluid saturation and substitution. *Geophysics*, *68*(2), 472–481.

Kim, D., & Lekic, V. (2019). Groundwater variations from autocorrelation and receiver functions. *Geophysical Research Letters*.

Larose, E., Carrière, S., Voisin, C., Bottelin, P., Baillet, L., Guéguen, P., ... others (2015). Environmental seismology: What can we learn on earth surface processes with ambient noise? *Journal of Applied Geophysics*, *116*, 62–74.

Lecocq, T., Caudron, C., & Brenguier, F. (2014). Msnoise, a python package for monitoring seismic velocity changes using ambient seismic noise. *Seismological Research Letters*, *85*(3), 715–726.

Lecocq, T., Longuevergne, L., Pedersen, H. A., Brenguier, F., & Stammler, K. (2017). Monitoring ground water storage at mesoscale using seismic noise: 30 years of continuous observation and thermo-elastic and hydrological modeling. *Scientific reports*, *7*(1), 14241.

Lin, F.-C., Moschetti, M. P., & Ritzwoller, M. H. (2008). Surface wave tomography of the western united states from ambient seismic noise: Rayleigh and love wave phase velocity maps. *Geophysical Journal International*, *173*(1), 281–298.

Lumley, D., King, A., Pevzner, R., Bona, A., Dautriat, J., Esteban, L., ... Urosevic, M. (2015). *Feasibility and Design for Passive Seismic Monitoring at the SW Hub CO2 Geosequestration Site: Australian National Low Emissions Council (ANLEC) R&D Project Number7-0212-0203.* University of Western Australia, Australia.

Mainsant, G., Larose, E., Brönnimann, C., Jongmans, D., Michoud, C., & Jaboyedoff, M. (2012). Ambient seismic noise monitoring of a clay landslide: Toward failure prediction. *Journal of Geophysical Research: Earth Surface*, *117*(F1).

Mao, S., Campillo, M., van der Hilst, R. D., Brenguier, F., Stehly, L., & Hillers, G. (2019). High temporal resolution monitoring of small variations in crustal strain by dense seismic arrays. *Geophysical Research Letters*, *46*(1), 128–137.

Minato, S., Tsuji, T., Ohmi, S., & Matsuoka, T. (2012). Monitoring seismic velocity change caused by the 2011 tohoku-oki earthquake using ambient noise records. *Geophysical Research Letters*, *39*(9).

Nakata, N., Gualtieri, L., & Fichtner, A. (2019). *Seismic ambient noise.* Cambridge University Press.

Obermann, A., Froment, B., Campillo, M., Larose, E., Planes, T., Valette, B., ... Liu, Q. (2014). Seismic noise correlations to image structural and mechanical changes associated with the mw 7.9 2008 wenchuan earthquake. *Journal of Geophysical Research: Solid Earth*, *119*(4), 3155–3168.

Poli, P., Campillo, M., Pedersen, H., Group, L. W., et al. (2012). Body-wave imaging of earth's mantle discontinuities from ambient seismic noise. *Science*, *338*(6110), 1063–1065.

Richter, T., Sens-Schönfelder, C., Kind, R., & Asch, G. (2014). Comprehensive observation and modeling of earthquake and temperature-related seismic velocity changes in northern chile with passive image interferometry. *Journal of Geophysical Research: Solid Earth*, *119*(6), 4747–4765.

Roberts, D. G., & Bally, A. W. (2012). *Regional geology and tectonics: Principles of geologic analysis* (Vol. 1). Elsevier.

Santamarina, J. C., Rinaldi, V. A., Fratta, D., Klein, K. A., Wang, Y.-H., Cho,

G. C., & Cascante, G. (2005). A survey of elastic and electromagnetic properties of near-surface soils. *Near-surface geophysics*, *1*, 71–87.

Saygin, E., & Kennett, B. (2012). Crustal structure of australia from ambient seismic noise tomography. *Journal of Geophysical Research: Solid Earth*, *117*(B1).

Saygin, E., & Kennett, B. L. (2010). Ambient seismic noise tomography of australian continent. *Tectonophysics*, *481*(1-4), 116–125.

Sens-Schönfelder, C., & Wegler, U. (2006). Passive image interferometry and seasonal variations of seismic velocities at merapi volcano, indonesia. *Geophysical research letters*, *33*(21).

Shapiro, N. M., Campillo, M., Stehly, L., & Ritzwoller, M. H. (2005). High-resolution surface-wave tomography from ambient seismic noise. *Science*, *307*(5715), 1615–1618.

Stalker, L., Varma, S., Van Gent, D., Haworth, J., & Sharma, S. (2013). South west hub: a carbon capture and storage project. *Australian Journal of Earth Sciences*, *60*(1), 45–58.

Tsai, V. C. (2011). A model for seasonal changes in gps positions and seismic wave speeds due to thermoelastic and hydrologic variations. *Journal of Geophysical Research: Solid Earth*, *116*(B4).

Yang, W., Wang, B., Yuan, S., & Ge, H. (2018). Temporal variation of seismic-wave velocity associated with groundwater level observed by a downhole airgun near the xiaojiang fault zone. *Seismological Research Letters*, *89*(3), 1014–1022.

Yates, A., Savage, M., Jolly, A., Caudron, C., & Hamling, I. (2019). Volcanic, coseismic, and seasonal changes detected at white island (whakaari) volcano, new zealand, using seismic ambient noise. *Geophysical Research Letters*, *46*(1), 99–108.